

## Measurements of the Recombination of Electrons with $\text{H}_3\text{O}^+ \cdot (\text{H}_2\text{O})_n$ -Series Ions\*

M. T. Leu, Manfred A. Biondi, and R. Johnsen

*Department of Physics, University of Pittsburgh, Pittsburgh, Pennsylvania 15213*

(Received 31 July 1972)

Recombination coefficients of electrons with ions of the hydrated hydronium-ion series  $\text{H}_3\text{O}^+ \cdot (\text{H}_2\text{O})_n$ , where  $n=0, 1, 2, 3, 4, 5, 6$ , have been determined with a microwave afterglow/mass-spectrometer apparatus. Afterglow measurements of electron density decays in helium-water-vapor mixtures are correlated with the decay of mass-identified ion currents to the wall of the microwave cavity. By varying the temperature of the gas and the partial pressure of the water vapor in the mixture, different groups of hydronium-series ions are made to dominate the afterglow. The measured recombination coefficients, in units of  $10^{-6} \text{ cm}^3/\text{sec}$ , are given. The implications of these results concerning ionization levels in the  $D$  region of the ionosphere are discussed.

### I. INTRODUCTION

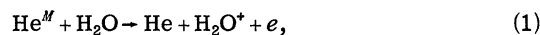
Direct mass-spectrometric determinations of the ion composition in the Earth's upper atmosphere by Narcisi<sup>1</sup> and co-workers have shown that the dominant ion species in the lower  $D$  region are the hydronium ion and its hydrates,  $\text{H}_3\text{O}^+ \cdot (\text{H}_2\text{O})_n$ , with  $n$  ranging from 0 to 3. The most abundant ion seems to be the first hydrate, i. e.,  $37^+$ . More recently, evidence for the presence of higher hydrates ( $n=4, 5$ ) in significant concentrations has been obtained from a rocket measurement by Johannessen and Krankowsky.<sup>2</sup>

Reaction sequences leading to hydrated hydronium ions have been suggested by Ferguson *et al.*<sup>3</sup> and Good *et al.*,<sup>4</sup> and many of the relevant ion-molecule rate constants have been determined in the laboratory.<sup>4,5</sup> However, attempts to combine laboratory measurements and ionospheric observations in order to obtain a consistent description of the  $D$ -region electron and ion height distributions have not been entirely successful so far. For example, an extremely high value for the electron-ion recombination coefficient of hydrated hydronium ions was required in one model<sup>6</sup> to obtain agreement with observations.

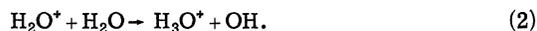
Since further reactions, such as charge transfer between the hydrated hydronium ions and the ambient neutrals, are not energetically possible, electron-ion recombination is expected to be the principal mechanism for removal of these ions. Consequently, to provide a more accurate assessment of the effect of the presence of these ions on  $D$ -region electron and ion concentrations, we have undertaken a series of laboratory measurements to determine the electron-ion recombination coefficients of the hydronium series ions  $19^+$ ,  $37^+$ ,  $55^+$ ,  $73^+$ ,  $91^+$ ,  $109^+$ , and  $127^+$ .

### II. APPARATUS AND MEASURING TECHNIQUES

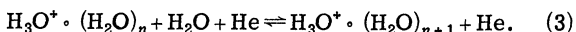
A microwave apparatus is used to study the loss of electrons and hydronium-series ions during the afterglow phase of a plasma generated in a helium-water-vapor mixture. The principal steps leading to formation of hydronium-series ions in the plasma afterglow are evidently metastable atom formation by electron impact on the helium buffer gas, followed by Penning ionization of water vapor by the reaction



followed by the fast two-body ion-molecule reaction<sup>7</sup>



The hydrated ions are then formed by a sequence of three-body collisions of the type



The microwave-afterglow/mass-spectrometer apparatus used in the present studies has been described in detail previously<sup>8,9</sup> and will be discussed only briefly here. Figure 1 is a simplified diagram of our experimental apparatus. Water vapor and ultrahigh-purity helium acting as a buffer gas are admitted to the copper microwave cavity by means of an ultrahigh-vacuum gas-handling system. The distilled water is contained in a small Pyrex glass bulb, and dissolved gases are removed prior to use by prolonged evacuation by a separate pumping system. A plasma containing hydronium ions and electrons is generated by means of a microwave pulse lasting 40  $\mu\text{sec}$  from a high-power magnetron with a repetition rate of 10  $\text{sec}^{-1}$ .

A fraction of the ions which diffuse to the cavity wall and effuse through a small sampling orifice

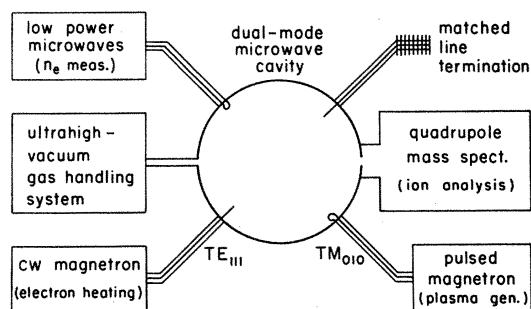


FIG. 1. Simplified block diagram of microwave afterglow/mass-spectrometer apparatus used in the recombination studies.

enter a differentially pumped quadrupole mass spectrometer where they are mass identified. The ion counts at each afterglow time interval are coherently summed over many cycles by means of a multichannel analyzer operating in a multiscaling mode. In this manner, the decays of the various positive ion wall currents are determined during the afterglow.

The principal measurement from which recombination coefficients are determined in these studies is that of the electron density as a function of afterglow time. The presence of free electrons within a microwave cavity changes its angular resonant frequency  $\omega$  from the empty value  $\omega_0$ . The frequency shifts  $\Delta\omega(t)$  are used to calculate the "microwave-averaged" electron density  $\bar{n}_{\mu w}(t)$  defined by

$$\bar{n}_{\mu w}(t) \equiv \frac{\int_{\text{vol}} n_e(\vec{r}, t) E_p^2(\vec{r}) dV}{\int_{\text{vol}} E_p^2(\vec{r}) dV} = C[1 + (\nu_{\text{eff}}/\omega)^2] \Delta\omega(t), \quad (4)$$

where  $n_e(\vec{r}, t)$  is the electron density,  $E_p(\vec{r})$  is the microwave probing electric field,  $C$  is a coefficient involving a group of physical constants, and  $\nu_{\text{eff}}$  is the effective electron-helium collision frequency.<sup>10</sup> For electron energies less than 0.2 eV, the electron-helium momentum-transfer cross section is independent of energy. In this case  $\nu_{\text{eff}}$  is given by

$$\nu_{\text{eff}} = \frac{4}{3} \bar{\nu}_c, \quad (5)$$

where  $\bar{\nu}_c$  represents the collision frequency averaged over the electron velocity distribution. The use of helium buffer at pressures approaching 40 Torr necessitates a  $\sim 10$ – $25\%$  correction of the electron densities determined from the frequency shifts compared to the low-pressure case ( $\nu_{\text{eff}} \ll \omega$ ).

In the present experiment, the  $TE_{111}$  electron heating mode shown in Fig. 1 has not been used.

### III. METHOD OF DATA ANALYSIS

During the afterglow, when the electrons and ions reach stationary energy distributions (e.g.,  $T_e = T_i = T_{\text{gas}}$ ), the variation of electron concentration is governed by the general continuity equation

$$\frac{\partial n_e}{\partial t} = \sum_j P_j - \sum_l L_l - \nabla \cdot \vec{\Gamma}_e, \quad (6)$$

where the  $P_j$  represent rates of electron production by various processes and may often be taken as zero during the afterglow and the  $L_l$  represent volume loss rates of electrons such as by recombination with positive ions and attachment to neutral molecules. The electron particle current density  $\vec{\Gamma}_e$  results from ambipolar diffusion of the electrons in response to electron and ion concentration gradients in the plasma afterglow.

If all other processes during the afterglow are negligible compared to recombination of electrons with various species of ions of concentrations  $n_{im}$  and recombination coefficients  $\alpha_m$ , the continuity equation may be approximated by

$$\frac{\partial n_e}{\partial t} \approx -n_e \sum_m \alpha_m n_{im}. \quad (7)$$

In the simplest case, i.e., an afterglow containing but a single species of positive ion, charge neutrality requires that  $n_e \approx n_i$ , and the solution of Eq. (4) is the well-known "recombination decay"

$$1/n_e(t) = 1/n_e(0) + \alpha t. \quad (8)$$

In this case the recombination coefficient  $\alpha$  is determined directly from the slope of a  $1/n_e(t)$ -vs- $t$  curve.

In the hydronium-ion studies it is very difficult to achieve conditions where a single ion species dominates throughout the afterglow. In most cases at least two species of ions are present in significant numbers. For this reason we have had to adopt several different methods of data analysis for the various regimes of the experiments. Empirically, two important cases are found which involve the presence of two ion species.

*Case 1.* The two species decay at different rates. The concentration of one species  $n_1$  is significantly greater than that of the second species  $n_2$ , which decays approximately exponentially with a time constant  $\tau_2$ , starting from an initial value  $n_2(0)$ . Equation (7) then becomes

$$\frac{\partial n_e}{\partial t} = -[\alpha_1 n_1 + \alpha_2 n_2(0) e^{-t/\tau_2}] n_e. \quad (9)$$

Again we invoke charge neutrality,  $n_e \approx n_1 + n_2$ , and find for the solution of Eq. (9),

$$\frac{1}{n_e(t)} = \frac{1}{g(t)} \left( \frac{1}{n_e(0)} + \alpha_1 \int_0^t g(t) dt \right), \quad (10)$$

where

$$g(t) = \exp [n_2(0) (\alpha_1 - \alpha_2) \tau_2 (1 - e^{-t/\tau_2})]. \quad (11)$$

A fit of Eq. (10) to the measured electron density decay, using  $\alpha_1$  as the parameter to be determined, can be obtained provided that one has information concerning the value of  $\alpha_2$  from other measurements.

*Case 2.* One of the hydronium-series ions and the next higher hydrate decay in apparent chemical equilibrium, maintaining a constant concentration ratio  $R \equiv n_2/n_1$  through reactions of the form of Eq. (3). In this case the solution of Eq. (7) is of a recombination-decay form [Eq. (8)], with  $\alpha$  replaced by an effective recombination coefficient defined by

$$\alpha_{\text{eff}} \equiv (\alpha_1 + R \alpha_2)/(1 + R). \quad (12)$$

Since  $R$  can be varied by changing the water-vapor concentration, determinations of  $\alpha_{\text{eff}}$  from the electron density decay curves as a function of  $R$  can be used to evaluate  $\alpha_1$  and  $\alpha_2$  (the intercept at  $R=0$  is  $\alpha_1$ ; the limiting value for large  $R$  is  $\alpha_2$ ).

The solutions for the electron decay obtained so far refer to the density at a point in space, while the microwaves measure  $\bar{n}_{\mu w}(t)$ , a spatial average of the electron density over the afterglow volume. It has been shown<sup>11,12</sup> that solutions similar in form to Eq. (8) are obtained for the spatially averaged case, i. e.,

$$1/\bar{n}_{\mu w}(t) = 1/\bar{n}_{\mu w}(0) + S\alpha t, \quad (13)$$

where  $S$  is a correction factor needed to obtain  $\alpha$  from the slope of the  $1/\bar{n}_{\mu w}(t)$ -vs- $t$  curves. This correction factor accounts for the effect of ambipolar diffusion on the spatial distribution of the electrons in the plasma afterglow and was obtained<sup>11,12</sup>

by computer solution of the continuity equation for electrons and a single ion species,

$$\partial n_e(\vec{r}, t)/\partial t = -\alpha n_e^2(\vec{r}, t) + D_a \nabla^2 n_e(\vec{r}, t), \quad (14)$$

where  $D_a$  is the ambipolar diffusion coefficient. We have applied the correction factors derived for this single-ion case to the more complicated two-ion cases just discussed. We use the average of the (nearly equal) ambipolar diffusion coefficients for neighboring ions of the hydronium series<sup>13</sup> and the effective recombination coefficient to determine the  $\beta$  correction.<sup>11,12</sup> Fortunately, in our microwave cavity, whose fundamental diffusion length  $\Lambda$  is 1.3 cm, the corrections are small, amounting to approximately 10%.

#### IV. RESULTS

The concentrations of the various hydrates of the hydronium ions are a sensitive function of gas temperature and, to a lesser extent, of the  $\text{H}_2\text{O}$ -vapor concentration. Only at high temperatures were we able to study the unclustered ion  $\text{H}_3\text{O}^+$  ( $19^+$ ), while it required dry-ice temperatures ( $\sim 200^\circ\text{K}$ ) to obtain substantial concentrations of the higher hydrates such as  $109^+$ . Thus, we have used the gas temperature as a means of controlling the ion species under investigation rather than of determining the temperature dependence of the recombination coefficient of a particular ion.

##### A. $540^\circ\text{K}$ Data

By heating the cavity to a temperature of  $540^\circ\text{K}$  and using a rather low water-vapor pressure of  $9 \times 10^{-5}$  Torr, the unclustered ion  $19^+$  was made dominant. As may be seen in Fig. 2(b), the ion wall

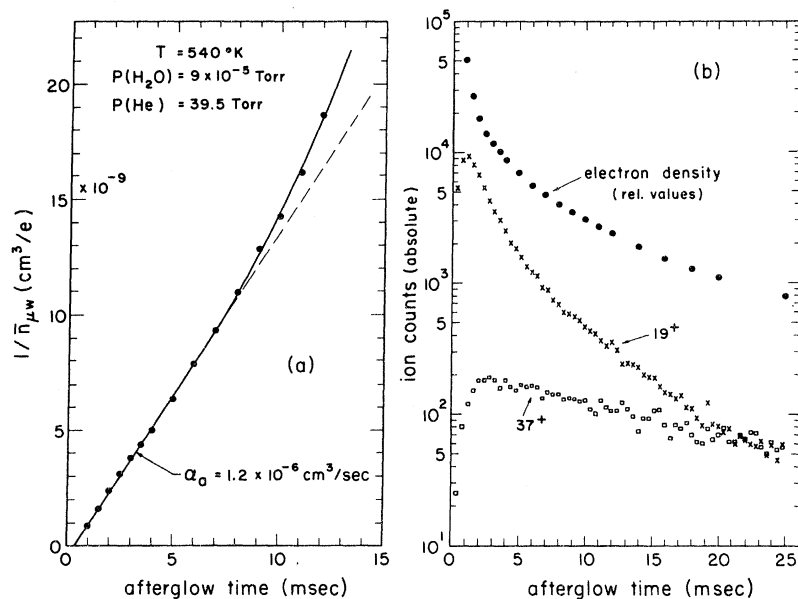


FIG. 2. (a) Recombination plot of electron density decay for case 1 conditions (see text). (b) Comparison of electron density and ion wall current decays under conditions where the ion  $19^+$  dominates the ion composition.

current for  $37^+$  is less than that for  $19^+$  for times less than  $\sim 20$  msec in the afterglow. A recombination decay, i. e., a linear increase in  $1/\bar{n}_{\mu w}$  with afterglow time, is observed over a factor of 12 in electron density. At later times the curve turns upward because of the increasing ratio of  $37^+$  to  $19^+$  and the increasing importance of ambipolar diffusion loss of electrons. The slope of the straight line in Fig. 2(a) yields an apparent recombination coefficient  $\alpha_a = 1.2 \times 10^{-6}$  cm<sup>3</sup>/sec.

These data fit the category of case 1 described in Sec. III. Therefore we have used Eq. (10), together with the measured  $37^+$  wall current exponential decay and the value  $\alpha(37^+) = 2.0 \times 10^{-6}$  cm<sup>3</sup>/sec (see below and Sec. IV B), to fit the observed electron density decay for afterglow times  $> 2$  msec, treating the recombination coefficient  $\alpha(19^+)$  as a parameter. [We have assumed that the mass-spectrometer ion currents are proportional to the ion concentrations in the afterglow and have used the measured  $37^+/19^+$  ion current ratio at 3 msec, together with the charge neutrality condition  $n_e \approx n_1 + n_2$ , to find  $n_2(0)$  for Eq. (11).] The best fit to the measurement yields the value  $\alpha(19^+) = 1.0 \times 10^{-6}$  cm<sup>3</sup>/sec.

We have been unable to study the ion  $19^+$  in the absence of all other ions, since a reduction in H<sub>2</sub>O-vapor concentration below  $\sim 9 \times 10^{-5}$  Torr to eliminate  $37^+$  leads to the appearance of He<sup>+</sup> and He<sub>2</sub><sup>+</sup> (from the buffer gas) and H<sub>2</sub>O<sup>+</sup> from the initial Penning-ionization step, as well as OH<sup>+</sup> and impurity ions.

As the H<sub>2</sub>O-vapor pressure is increased, first the ion  $37^+$  begins to dominate the afterglow (at  $\sim 5 \times 10^{-3}$  Torr) and then  $55^+$  dominates (at  $\sim 0.5$

Torr). Using the analysis based on Eq. (10), we obtain values for these ions of  $\alpha(37^+) = 2.0 \times 10^{-6}$  cm<sup>3</sup>/sec and  $\alpha(55^+) = 4.0 \times 10^{-6}$  cm<sup>3</sup>/sec from curve fitting of the electron density decay data at 540 °K.

### B. 415 °K Data

At a gas temperature of 415 °K and H<sub>2</sub>O-vapor pressure of  $\sim 5 \times 10^{-3}$  Torr, the ions  $55^+$  and  $37^+$  are observed to decay together, maintaining a constant concentration ratio throughout most of the afterglow [see Fig. 3(b)]. Further, the electrons and ions decay together, as indicated by the dashed lines on the ion curves which are renormalized electron density values. These data fit case 2 of Sec. III and have been analyzed in terms of an effective  $\alpha$ , Eq. (12). The corrected slope in Fig. 3(a) yields a value  $\alpha_{\text{eff}} = 3.9 \times 10^{-6}$  cm<sup>3</sup>/sec from a curve that is linear over an electron density range of  $\sim 50$ .

Values of  $\alpha_{\text{eff}}$  were obtained as a function of  $R \equiv [55^+]/[37^+]$  for the range  $0.1 \leq R \leq 7$  by varying the water-vapor pressure from  $2.3 \times 10^{-4}$  to  $1.7 \times 10^{-2}$  Torr. At the highest water concentrations the effect of the ion  $73^+$  became noticeable, necessitating a correction to the data by an extension of the  $\alpha_{\text{eff}}$  analysis. The observed  $\alpha_{\text{eff}}$  values are shown by the crosses in Fig. 4. The solid curve represents the variation of  $\alpha_{\text{eff}}$  with  $R$  predicted by Eq. (12) when the effect of the  $73^+$  ion is included, while the dashed curve represents the curve when only the ions  $55^+$  and  $37^+$  are considered. The values that give this degree of fit are  $\alpha(37^+) = 2.2 \times 10^{-6}$  cm<sup>3</sup>/sec and  $\alpha(55^+) = 4.2 \times 10^{-6}$  cm<sup>3</sup>/sec. [The value  $\alpha(73^+) = 4.9 \times 10^{-6}$  cm<sup>3</sup>/sec, obtained in Sec. IV C, was also used.]

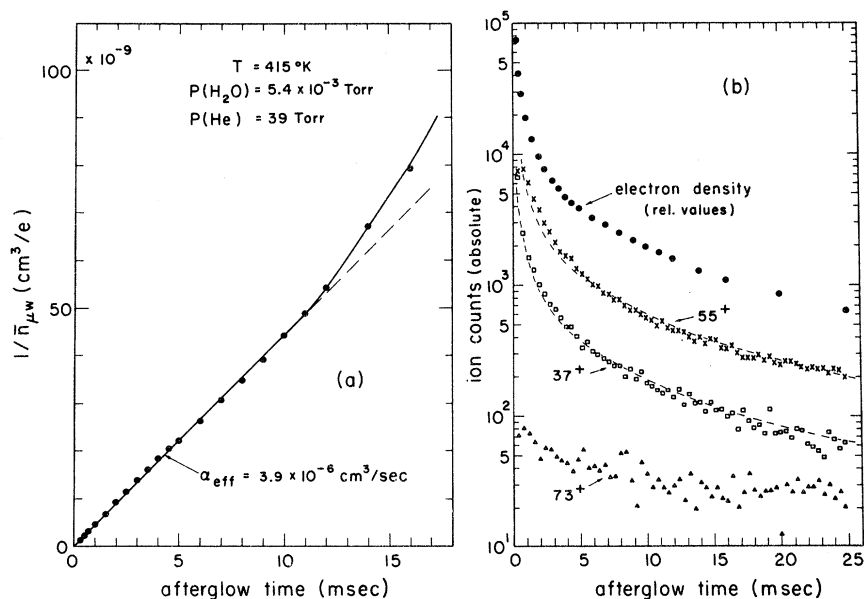


FIG. 3. (a) Recombination plot for electron decay under effective recombination coefficient conditions, case 2. (b) Comparison of electron density and ion wall current decays under conditions where the ions  $55^+$  and  $37^+$  decay in apparent equilibrium (together with a small amount of the ion  $73^+$ ). The dashed lines through the  $37^+$  and  $55^+$  data are scaled values of the electron density normalized to the curves at 5 msec.

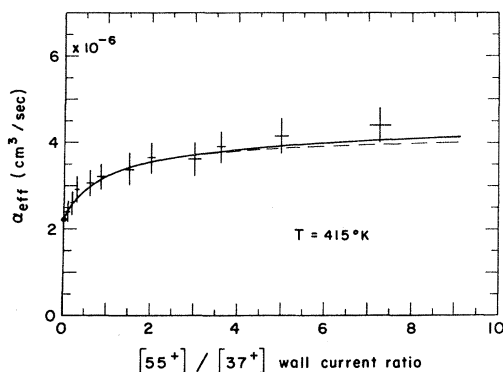


FIG. 4. Effective recombination coefficient  $\alpha_{\text{eff}}$  for different  $[55^+]/[37^+]$  wall current ratios (measured at 4 msec in the afterglow). The dashed line is a fit of the data to Eq. (12), while the solid line includes a correction for the effect of the ion  $73^+$ .

#### C. 300 °K Data

As in Sec. IV B, ion decays in apparent chemical equilibrium were noted for the ions  $73^+$  and  $55^+$ , with other ions present in small amounts. Values of  $\alpha_{\text{eff}}$  as a function of  $R \equiv [73^+]/[55^+]$  were obtained over the range  $0.8 \leq R \leq 16$  by varying the water-vapor pressure from  $5 \times 10^{-4}$  to  $2 \times 10^{-2}$  Torr. From a curve similar in form to that of Fig. 4, the values  $\alpha(55^+) = 3.8 \times 10^{-6}$  cm<sup>3</sup>/sec and  $\alpha(73^+) = 4.9 \times 10^{-6}$  cm<sup>3</sup>/sec were deduced at 300 °K.

#### D. 205 °K Data

The abundance of the higher hydrates increased dramatically when the gas temperature was lowered to 205 °K by surrounding the microwave cavity with dry ice. However, in these low-temperature studies it was no longer possible to find conditions where only two ions species were present in significant amounts. An example of the relative concentrations of  $73^+$  through  $145^+$  is shown in the inset of Fig. 5. These ions all decayed together during the afterglow in apparent equilibrium, suggesting that the electron density should follow a recombination decay controlled by a more general effective recombination coefficient,

$$\alpha_{\text{eff}} = \frac{\alpha_1 + R_{21} \alpha_2 + R_{31} \alpha_3 + R_{41} \alpha_4 + \dots}{1 + R_{21} + R_{31} + R_{41} + \dots}, \quad (15)$$

where  $R_{21} = n_2/n_1$ , etc.

As will be seen from the  $1/\bar{n}_{ew}$ -vs- $t$  measurements in Fig. 5, the recombination decay is obeyed over a range of  $\sim 40$  in electron density, leading to a value  $\alpha_{\text{eff}} = 8.1 \times 10^{-6}$  cm<sup>3</sup>/sec from the corrected slope of the curve. Measurements of  $\alpha_{\text{eff}}$  were made for many different concentrations of H<sub>2</sub>O vapor to vary the ratios of the several ions. From an analysis of these data the following estimates

were obtained:  $\alpha(91^+) = 6.0 \times 10^{-6}$ ,  $\alpha(109^+) = 7.5 \times 10^{-6}$ ,  $\alpha(127^+) \leq 10 \times 10^{-6}$  cm<sup>3</sup>/sec at 205 °K.

#### V. DISCUSSION AND CONCLUSIONS

The results of the measurements are summarized in Table I, which includes our estimate of the random and the systematic errors encountered in the various cases. Inasmuch as we were unable to study a single ion species at a time, uncertainties in the relative concentrations of the ions can lead to uncertainties in the deduced  $\alpha$  values. We have used the ion counting rates as measured by the quadrupole mass spectrometer to provide relative values of the ion concentrations in the afterglow. This means that we have neglected effects due to the slightly different ambipolar diffusion coefficients of the various ions and have also neglected possible differences in the over-all transmission of the quadrupole mass spectrometer and in the secondary-electron emission characteristics of the channeltron electron multiplier. We justify this neglect empirically by the observation that the measured  $\alpha_{\text{eff}}$ -vs- $R$  curves such as is shown in Fig. 4 follow the theoretical form without adjustment of the measured ion wall current ratios.

The recombination coefficients determined from the  $\alpha_{\text{eff}}$  analysis for two ion species (case 2) are probably least affected by possible errors in the concentrations of the ions, since  $\alpha_1$  may be determined from an extrapolation of the  $\alpha_{\text{eff}}$  values to  $R=0$  and  $\alpha_2$  determined at large values of  $R$ , neither of which requires accurate absolute values of  $R$ . In the case of the independently decaying ions (case 1) and in the multiple ion species  $\alpha_{\text{eff}}$  analysis, larger uncertainties are assigned to the deduced values because of the interdependence of the value deduced for one ion on that deduced for another. Uncertainties in the diffusion corrections to the recombination curves<sup>11,12</sup> resulting from im-

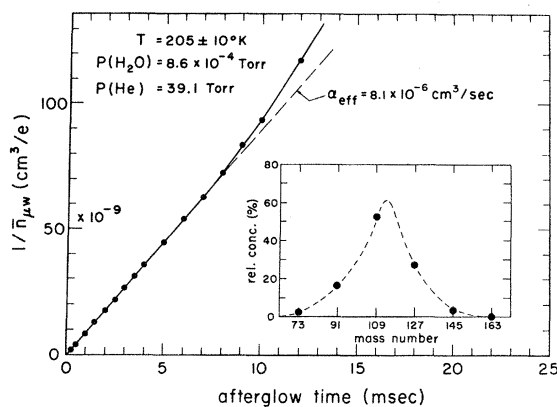


FIG. 5. Recombination plot of electron density decay at 205 °K. Inset: Relative concentrations of the ions  $73^+$  to  $145^+$ , which decay together in apparent equilibrium.

TABLE I. Electron-ion recombination coefficients for hydrated hydronium ions in units of  $10^{-6}$  cm<sup>3</sup>/sec.

| Ion<br>T(°K) | 19*       | 37*       | 55*       | 73*       | 91*       | 109*      | 127* |
|--------------|-----------|-----------|-----------|-----------|-----------|-----------|------|
| 540          | 1.0 ± 0.2 | 2.0 ± 0.3 | 4.0 ± 0.6 | ...       | ...       | ...       | ...  |
| 415          | ...       | 2.2 ± 0.4 | 4.2 ± 0.6 | ...       | ...       | ...       | ...  |
| 300          | ...       | ...       | 3.8 ± 0.6 | 4.9 ± 0.8 | ...       | ...       | ...  |
| 205          | ...       | ...       | ...       | ...       | 6.0 ± 1.2 | 7.5 ± 1.5 | ≤ 10 |

perfect knowledge of the initial spatial distribution of the electrons in the cavity may lead to a  $\sim \pm 5\%$  error in the recombination coefficient determination in a typical case. All other sources of error, such as uncertainties in the electron densities due to collision-frequency corrections of the frequency-shift data, are small ( $\lesssim 1\%$ ).

The simple ion  $H_3O^+$  exhibits a rather large coefficient at 540 °K,  $\alpha(19^*) = (1.0 \pm 0.2) \times 10^{-6}$  cm<sup>3</sup>/sec. Using the  $T^{-1/2}$  temperature dependence predicted theoretically for simple ions at temperatures where the molecular ions are principally in their ground vibration state, we expect a value at room temperature (300 °K) of  $\sim 1.3 \times 10^{-6}$  cm<sup>3</sup>/sec and at *D*-region temperatures ( $\sim 200$  °K) of  $\sim 1.6 \times 10^{-6}$  cm<sup>3</sup>/sec. Our measured value at 540 °K may be compared with the result at 2100 °K of Green and Sugden,<sup>14</sup> who determined a value of  $2 \times 10^{-7}$  cm<sup>3</sup>/sec from mass-identified ion current decays from a hydrogen-oxygen-acetylene flame. It may also be compared with the results of Wilson and Evans,<sup>15</sup> who used microwaves to measure the electron density decays behind shock fronts in argon containing small amounts of oxygen and a hydrocarbon such as acetylene. They found that the recombination coefficient varied approximately as  $T^{-2}$  over the range  $2400 \leq T \leq 5600$  °K, with a value  $\alpha = 1.5 \times 10^{-7}$  cm<sup>3</sup>/sec at 3000 °K. Although no mass analysis was used, the principal ion in these studies was expected to be  $H_3O^+$ . To compare these values with our results at 540 °K, we should use a temperature variation as  $T^{-1/2}$  for low temperatures (less than  $\sim 1000$  °K) going over to the high-temperature  $T^{-2}$  variation. In this case, the flame and shock-front results are compatible with our 540 °K value.

Although the recombination coefficient for the simple ion  $H_3O^+$  appears to exhibit a substantial temperature variation of the type expected for dissocia-

tive recombination, the recombination coefficient of the clustered ion  $H_3O^+ \cdot (H_2O)_2$  exhibits no detectable variation with temperature within the  $\pm 15\%$  measurement uncertainty over the range  $300 \leq T \leq 540$  °K (see Table I). This weaker temperature dependence suggests that a modified form of dissociative recombination may apply to these complex clustered ions. The very large recombination coefficient,  $\alpha(55^*) = 4 \times 10^{-6}$  cm<sup>3</sup>/sec, may result from excitation of internal modes (e. g., rotation) of the complex ion as part of the initial capture step, thus lengthening the time for autoionization and assuring stabilization by dissociation.

It will be seen from Table I that, at a given temperature, there appears to be a systematic increase in the recombination coefficients with increasing number of water clusters on the  $H_3O^+$  core. As mentioned in Sec. I, attempts to account for the sharp decrease in electron density at the altitude in the *D* region where hydronium-series ions occur have led to use of recombination coefficients well in excess of  $10^{-5}$  cm<sup>3</sup>/sec. While it is at least conceivable that the very heavy clusters,  $n = 10$ , might have coefficients approaching these values, the suggestion that these weakly bound clusters are present in the *D* region, but have not been detected, does not appear to us to be tenable. Using the equilibrium constants of Kebarle *et al.*<sup>16</sup> and as low a temperature (180 °K) and as high a concentration of water vapor ( $\sim 10^9$  cm<sup>-3</sup>) as seem possible for the 85-km level of the atmosphere, we find that the principal ion should be 91\* if there is time for the concentrations of the various ions to reach chemical equilibrium (i. e., recombination loss is neglected). Since  $\alpha(91^*) = 10^{-6}$  cm<sup>3</sup>/sec, it appears that a recombination coefficient  $\lesssim 5 \times 10^{-6}$  cm<sup>3</sup>/sec, rather than one exceeding  $10^{-5}$  cm<sup>3</sup>/sec, is appropriate to the hydronium-series ion layer of the *D* region.

\*Research supported in part by the U. S. Army Research Office, Durham, under Contract No. DA-ARO-D-31-124-76-G34.

<sup>1</sup>R. S. Narcisi, *Space Res.* **7**, 186 (1967).

<sup>2</sup>A. Johannessen and D. Krankowsky, *J. Geophys. Res.* **77**, 2888 (1972).

<sup>3</sup>E. E. Ferguson and F. C. Fehsenfeld, *J. Geophys. Res.* **74**, 5743 (1969).

<sup>4</sup>A. Good, D. A. Durden, and P. Kebarle, *J. Chem.*

*Phys.* **52**, 212 (1970).

<sup>5</sup>F. C. Fehsenfeld, M. Mosesman, and E. E. Ferguson, *J. Chem. Phys.* **55**, 2115 (1971).

<sup>6</sup>G. C. Reid, *J. Geophys. Res.* **75**, 2551 (1970).

<sup>7</sup>V. L. Tal'roze and E. L. Frankevich, *Zh. Fiz. Khim.* **34**, 2709 (1960).

<sup>8</sup>C. S. Weller and M. A. Biondi, *Phys. Rev.* **172**, 198 (1968).

<sup>9</sup>F. J. Mehr and M. A. Biondi, *Phys. Rev.* **181**, 264

(1969).

<sup>10</sup>I. P. Shkarofski, T. W. Johnston, and M. P. Bachynski, *The Particle Kinetics of Plasmas* (Addison-Wesley, Reading, Mass., 1966), p. 128ff.

<sup>11</sup>L. P. Gray and D. E. Kerr, *Ann. Phys. (N.Y.)* **17**, 276 (1962).

<sup>12</sup>L. Frommhold and M. A. Biondi, *Ann. Phys. (N.Y.)* **48**, 407 (1968).

<sup>13</sup>The alkali-ion mobility vs ion mass curve for helium [see, for example, H. S. W. Massey, *Electronic and Ionic Impact Phenomena* (Oxford U.P., London, 1971),

Vol. 3, p. 1961] was used to estimate the values for the ions 19<sup>+</sup>, 37<sup>+</sup>, 55<sup>+</sup>, etc. In support of this assumption, we have found that the mobilities of ions such as O<sub>2</sub><sup>+</sup> and N<sub>2</sub><sup>+</sup> fall on this curve.

<sup>14</sup>J. A. Green and T. M. Sugden, *Ninth Symposium on Combustion* (The Combustion Institute, Pittsburgh, Pa., 1963), p. 607.

<sup>15</sup>L. N. Wilson and E. W. Evans, *J. Chem. Phys.* **46**, 859 (1967).

<sup>16</sup>P. Kebarle, S. K. Searles, A. Zolla, J. Scarborough, and M. Arshadi, *J. Am. Chem. Soc.* **89**, 6393 (1967).

PHYSICAL REVIEW A

VOLUME 7, NUMBER 1

JANUARY 1973

## Self-Diffusion in Krypton at Intermediate Density

P. Carelli\* and I. Modena\*

*Laboratori Nazionali del Comitato Nazionale per l'Energia Nucleare, Frascati, Italy*

and

F. P. Ricci

*Istituto di Fisica "G. Marconi," Università di Roma,  
and Gruppo Nazionale Struttura della Materia del Consiglio Nazionale delle Ricerche,  
Roma, Italy*

(Received 1 May 1972)

The self-diffusion coefficient in Kr has been measured throughout a large range of densities ( $0.35 < \rho < 2 \text{ g/cm}^3$ ) at temperatures near the critical one. The results are compared with molecular-dynamic calculations and with the CH<sub>4</sub> behavior. Although the qualitative agreement is good, disagreement from a quantitative point of view was found. The "normal behavior" of the self-diffusion coefficient in the critical region has been deduced.

### INTRODUCTION

At present the "computer experiments"<sup>1</sup> seem to be the most powerful way for investigating the static and the dynamic behavior of the dense fluids. Some of the numerical predictions must, however, be compared with real experiments. This ensures that the hypothesis about the intermolecular potential on which the model is based gives a correct description of the world around us.

Recently a thorough study has been published<sup>2</sup> on the self-motion of atoms in a Lennard-Jones fluid; the study was carried out using computer experiments. These "experiments" have a range of  $0.72 \leq T^* \leq 5.09$  and  $0.30 \leq \rho^* \leq 0.85$ , where  $T^* = k_B T / \epsilon$  and  $\rho^* = \rho \sigma^3 / m$  are the reduced temperature and density,  $\epsilon$  and  $\sigma$  the depth and the core of the Lennard-Jones potential,  $m$  the atomic mass, and  $k_B$  the Boltzmann constant.

Noble gases Ar, Kr, and Xe are the substances which should be described by a classical Lennard-Jones fluid. The authors<sup>2</sup> compare the numerical results of the self-diffusion constant with some experiments on Ar<sup>3</sup> and claim a very good agreement. However, these experiments cover a small range of densities and temperatures since  $0.725 \leq T^* \leq 0.925$  and  $0.763 \leq \rho^* \leq 0.835$ ; that is, the

measurements are only near the triple point. Since suggestions have been made that at intermediate densities many-body forces become important, it is worthwhile to measure the self-diffusion coefficient in Kr for a large range of densities ( $0.1 \leq \rho^* \leq 0.7$ ). Moreover, if the experimental data are taken at a temperature near the critical temperature  $T_c$  but outside the critical region [i.e.,  $(T - T_c / T_c) > 3\%$ ], we obtain the "normal" behavior of the self-diffusion coefficient in the critical region. This point is quite important since the deduction of an anomalous behavior of the self-diffusion coefficient at the critical point depends upon a good knowledge of the "normal" behavior. This problem has caused erroneous statements in the past.<sup>4,5</sup> Finally, we wish to point out that extensive measurements are available for the self-diffusion in CH<sub>4</sub><sup>6</sup> at various temperatures and for  $0.07 \leq \rho^* \leq 0.82$ .

Since CH<sub>4</sub> is a polyatomic molecule, the comparison between the behavior of Kr and CH<sub>4</sub> will give us an idea of the importance of the internal degrees of freedom in the self-diffusion process.

### EXPERIMENTAL APPARATUS

The capillary method of Anderson and Saddington<sup>7</sup> has been used. Since we were interested in